Journal of Power Sources 244 (2013) 375–381

Contents lists available at SciVerse ScienceDirect

Journal of Power Sources

journal homepage: www.elsevier.com/locate/jpowsour

Preparation of nanocrystalline $LiMn_2O_4$ thin film by electrodeposition method and its electrochemical performance for lithium battery

Zhen Quan, Shouya Ohguchi, Masayasu Kawase, Hiroshi Tanimura, Noriyuki Sonoyama*

Department of Materials Science and Engineering, Nagoya Institute of Technology, Gokiso-cyo, Showa-ku, Nagoya 466-8555, Japan

HIGHLIGHTS

- The $LiMn_2O_4$ thin film was prepared by electrodeposition and sintering method.
- The particle size of $LiMn_2O_4$ thin film is ca. 50 nm
- For the preparation of nanoparticle, it does not need any special equipment.
- The $LiMn_2O_4$ thin film has good electric contact with substrate.
- Thinner $LiMn_2O_4$ films showed superior rate performance and good stability.

ARTICLE INFO

Article history:
Received 28 September 2012
Received in revised form
24 November 2012
Accepted 13 December 2012
Available online 27 December 2012

Keywords:
$LiMn_2O_4$ cathode
Lithium thin film battery
Electrodeposition
High rate discharge performance

ABSTRACT

The $LiMn_2O_4$ thin films composed of nanoparticles were synthesized by sintering electrodeposited Mn_3O_4 precursor on the Au substrate, and the electrochemical properties were investigated. The electrochemical performance was dependent on the film thickness. For the thinner $LiMn_2O_4$ films, cycling in the voltage range of 4.3 V–3.4 V resulted in superior rate performance, that is almost 100% of discharge capacity compared with that at 20 times of discharge current density, and good stability without capacity loss until 500 cycles. CV and EIS measurements revealed that $LiMn_2O_4$ thin film has good electric contact with substrate and high lithium diffusion coefficient of 10^{-9}–10^{-11} cm^2 s^{-1} could be obtained.

1. Introduction

Recently, lithium ion thin film batteries attracted much interest to the application for the back up power sources of microelectronic devices and micromechanics such as smart card, sensor technology, computer memory chip and so on. Among the cathode materials, $LiMn_2O_4$ is the promising candidate for the thin film battery, because the feature of low cost, environmentally benign and has 3D frame work that benefits for the Li ion diffusion [1,2]. The synthesis techniques of $LiMn_2O_4$ thin films have been reported by many groups, such as, sol–gel method [3,4], electrostatic spray deposition (ESD) [5,6], radio frequency (r.f.) magnetron sputtering [7,8] and pulse laser deposition (PLD) [9,10]. Usually, good electrochemical performance obtained by the $LiMn_2O_4$ thin film composed of nanoparticle, because small particle size leads short lithium ion diffusion length and large surface reaction area. For example, the $LiMn_2O_4$ thin film synthesized by PLD method that composed of extremely small particle (10–30 nm) maintained almost the same shape of discharge curve in the discharge rate range between 36 C and 720 C [11]. However, controlling the particle size to the nanometer level often needs vacuum deposition condition like r.f sputtering or PLD method, which directly raises the cost of fabrication.

Electrochemical deposition is another way to synthesis of thin film with the advantage of low synthesis temperature, low costs, and high purity in the product [12,13]. This method also enables rigid control of film thickness, uniformity and deposition rate. Moreover, the good electric contact between the film and substrate is expected, because the product directly formed on the substrate electrochemically. For example, Manganese dioxide cathodes synthesized by electrodeposition method are reported to show good electrochemical property for the application of super capacitors [14,15] and lithium batteries [16,17]. Recently, our group reported on the electrochemical property of $LiCoO_2$ thin film

* Corresponding author.Tel/fax: +81 52 735 7243.
E-mail addresses: sonoyama.noriyuki@nitech.ac.jp, sonoyama@nitech.ac.jp (N. Sonoyama).

0378-7753/$ – see front matter © 2012 Elsevier B.V. All rights reserved.
http://dx.doi.org/10.1016/j.jpowsour.2012.12.087

consisted with nanoparticle synthesized by electrophoretic deposition (EPD) and hydrothermal treatment. In spite of the low cost of fabrication, the $LiCoO_2$ thin film showed reversible charge–discharge ability even at 400 C discharge current [18].

In the present study, $LiMn_2O_4$ thin film composed of nanoparticle is attempted to synthesize by electrodeposition of manganese oxide precursor and subsequent sintering treatment, and its electrochemical properties of the thin film were investigated.

2. Experiment

Manganese oxide precursor was deposited on anode Au substrate in the potentiostatic mode with an Au sheet as counter electrode. The pH of electrolyte solution containing 3 mol L^{-1} $MnSO_4 \cdot 5H_2O$ (99%, Kishida chemical) was adjusted to be 2.3 by adding H_2SO_4 acid (98%, Kishida chemical), under flowing oxygen gas. Manganese oxide precursor film was electrodeposited on the Au substrate (1 cm × 1 cm × 0.01 cm) under the cathodic polarization of 1.7 V by oxidation of Mn^{2+} ion in the solution (kept at 40 °C). The film thickness was changed by controlling the electric charge flowed (5, 10, 50°mili-coulomb) under the control of potentio-galvanostat (Hokuto HABF 501). The precursor covered ca. 0.65 cm^2 on the surface of Au substrate. Then the films were rinsed with distilled water, dried at room temperature followed by dipping 0.03 M LiOH (99%, High purity chemical) solution on the surface of the films. The $LiMn_2O_4$ thin films were prepared through sintering manganese oxide thin films at 750 °C for 12 h under air atmosphere. The three as-prepared $LiMn_2O_4$ thin films with different film thickness were named as 5 mC, 10 mC, 50 mC, respectively, indicating the flowed electric charge of the electrodeposited precursor hereafter.

The crystal structure of the thin films was characterized by X-ray diffractometer (Ultima IV, Rigaku) using Cu Kα radiation and laser Raman spectrophotometer (NSR-3300, JASCO) using DPSS laser at the wavelength of 532 nm. Electrochemical quartz crystal microbalance (ECQCM) controller (HQ 101D, Hokuto) was employed to measure the mass of the precursor by directly depositing on the gold surface (1.33 cm^2) coated on AT cut quartz 6 MHz of crystal. The morphologies of thin films were observed by the scanning electron microscope (SEM) (S-4800, Hitachi). For electrochemical measurements, $LiMn_2O_4$ thin films on Au substrates were assembled in HS cell (Hohsen) with lithium metal as anode and 1 M solution of $LiPF_6$ in EC:DEC (3:7, v/v) as the electrolyte solution. The charge–discharge and CV measurements were performed on potentio-galvanostat (Solartron 1280C). The electrochemical impedance spectroscopy (EIS) measurement was carried out with an impedance analyzer (Solartron 1255) connected to potentiostat (Solartron 1280C) over the frequency range from 10^6 Hz to 10^{-2} Hz at cell voltage with the applied voltage of 10 mV. All of the electrochemical measurements were carried out at 25 °C.

3. Results and discussion

X-ray diffraction patterns for precursor and $LiMn_2O_4$ thin films were shown in Fig. 1. For the XRD measurement, the manganese oxide precursor thick film was deposited with flowing 250 mC of electric charge in order to increase the intensity of the reflection. However, only indistinct peaks near 40° and 42° were observed. It might be due to the extremely small particle size or amorphous nature of the precursor. For the thin films reacted with LiOH at 750 °C, three reflections appeared at 18°, 40°, 42° except the reflection of the Au substrate. The small reflection at 18° seems to be corresponding to the 111 reflection of spinel $LiMn_2O_4$ (ICSD No. 40485), but other reflections of spinel were too weak to confirm.

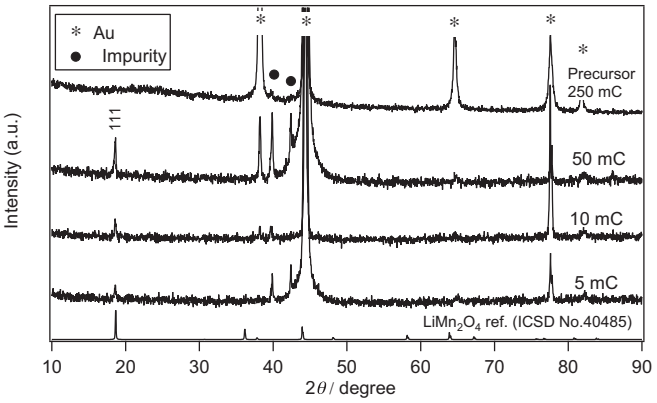

Fig. 1. The XRD patterns of the precursor and $LiMn_2O_4$ thin films with various film thickness.

The two sharp reflections at 40° and 42°, roughly agreed with MnO_2 phase. By Scherrer's equation, the crystallite sizes of the $LiMn_2O_4$ estimated from 111 reflection were 51.3, 55.7 and 52.3 nm, respectively. This result suggests that as-synthesized $LiMn_2O_4$ thin films composed of nanoparticle with the size of ca. 50 nm, and the particle size was independent from the electrodeposition time and thickness of precursor. Although the size of the $LiMn_2O_4$ nanoparticle obtained in this method was slightly bigger than 20–30 nm [11] compared with that synthesized by pulsed laser deposition method, it is much smaller than that of synthesized by other usual preparing roots, 100–200 nm for sol–gel method [4], 200 nm for laser spark atomizer method [19] or 10 μm for electrostatic spray deposition method [20]. In general, nano sized particle of the cathode thin film leads short Li^+ diffusion length and large surface area to facilitate lithium diffusion in the host phase, so the $LiMn_2O_4$ thin film prepared by sintering electrodeposited precursor is expected to derive high rate charge–discharge performance.

The Raman spectra of the precursor on Au that electrodeposited by flowing 5, 10 and 50 mC are shown in Fig. 2(a). For the precursor of 50 mC, a significant peak at 656 cm^{-1} and three smaller peaks at 309, 362, 478 cm^{-1} are indexed for the spinel structure of Mn_3O_4 with good agreement to the literature data [21,22]. Absence of Mn_3O_4 reflection in the XRD pattern of the precursor indicates that the Mn_3O_4 electrodeposited on the Au substrate is amorphous state. Two weak bands at 510 cm^{-1} and 569 cm^{-1} were near the signals attributed to Mn–O lattice vibration in MnO_2 [21]. The presence of MnO_2 in the precursor phase is consistent with the result of XRD measurement. Although the peak intensity of Raman spectra was weaken seriously, the similar pattern also observed in the precursor of 5 and 10 mC Fig. 2(b) displayed the Raman spectra of the thin film reacted with LiOH at 750 °C. All of the three thin films represented the same pattern with the similar peak intensity. The strongest band located at 623 cm^{-1} and two weak bands at 576 cm^{-1} and 480 cm^{-1} in accordance with the A_{1g} and F_{2g} modes of spinel $LiMn_2O_4$ [23]. Based on the XRD and Raman spectra, it is demonstrated that amorphous Mn_3O_4 and a little amount of MnO_2 with low crystallinity were electrodeposited on the Au substrate according to the reactions (1) and (2).

$$3Mn^{2+} + 4H_2O = Mn_3O_4\,(\text{amorphous}) + 8H^+ + 2e^- \quad (1)$$

$$Mn^{2+} + 2H_2O = MnO_2 + 4H^+ + 2e^- \quad (2)$$

In the sintering stage at air atmosphere, Mn_3O_4 reacted with LiOH to form $LiMn_2O_4$ though the MnO_2 remained as impurity and its crystallinity increased. Absence of other bands attributable to

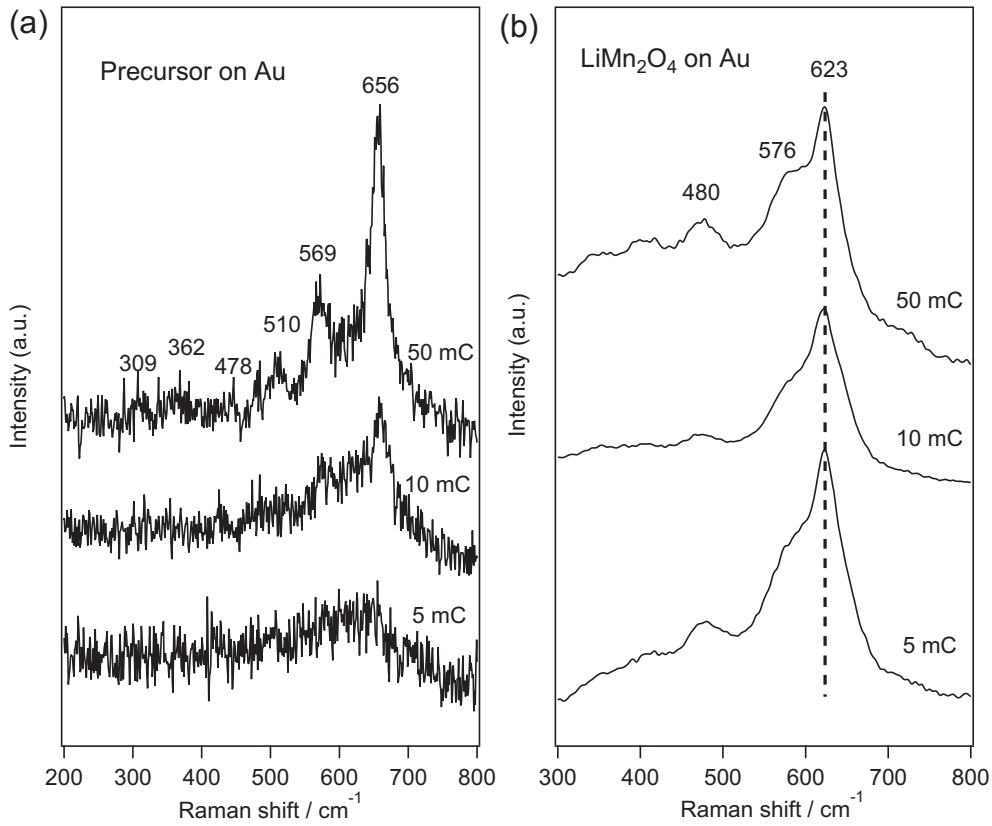

Fig. 2. The Raman spectra of (a) precursor and (b) $LiMn_2O_4$ thin films with various film thickness on Au substrate.

Mn_3O_4 or MnO_2 precursor in Fig. 2, indicates that the thin films mainly consist of $LiMn_2O_4$ nanoparticle and contain just a little amount of MnO_2 as impurity.

The mass of the precursor films with various thickness was carefully measured by QCM method. In order to obtain the film with same thickness, 2 times of electric charge, 10, 20, and 100 mC was flowed due to the twice area of gold surface on crystal (1.33 cm^2) of the each sample (0.65 cm^2) for the electrochemical measurement. The mass of manganese oxide precursor was calculated by Sauerbrey Eq. (3):

$$\Delta f = -\frac{2f_0^2}{A\sqrt{\rho\mu}}\cdot\Delta m \tag{3}$$

Where f_0 is resonant frequency (Hz), Δf is frequency change (Hz), Δm is mass of deposited precursor (g), A is active crystal area (1.33 cm^2), ρ is density of quartz (2.648 g cm^{-3}), μ is shear modulus of quartz for AT-cut crystal (2.947×10^{11} g cm^{-1} s^{-1}). We presumed that precursor film is composed of Mn_3O_4, and reacts with LiOH to form $LiMn_2O_4$ with 100% efficiency. The thickness of the thin film was roughly estimated from theoretical density of $LiMn_2O_4$ (4.3 g cm^{-3}). The obtained mass and thickness were shown in Table 1. Very thin films were obtained for 5 and 10 mC sample with the thickness of ~10 and ~20 nm. This very small film thickness will contribute in decreasing in the resistance that will benefit for the acceleration of lithium (de) intercalation. The mass of electrodeposited precursor was proportional to the flowed electric charge with the rate of 0.56 μg mC^{-1}.

Fig. 3 showed the surface morphologies of 5, 10, and 50 mC samples observed by SEM. For the 5 mC sample shown in Fig. 3(a), it was observed that very uniform thin films are covering on Au substrate surface. As deposition time increase, the thin film become thicker and denser as shown in Fig. 3(b) and (c). In addition, some aggregates of $LiMn_2O_4$ nanoparticles are distributed on the surface of 50 mC sample. These aggregates could hinder the smooth diffusion of Li^+ and increase the resistance of thin film.

The high rate discharge performance of $LiMn_2O_4$ thin films with various film thickness was shown in Fig. 4. The charge–discharge experiments performed with charge current of 10 μA and discharge current of 10, 100, 200 and 300 μA cm^{-2} at the voltage range of 3.5 V–4.3 V. In Fig. 4(a–c), two clear plateaus are appeared at 4.16 V and 4.0 V in the discharge curves plotted at discharge current of 10 μA cm^{-2} for the three samples. These two plateaus were characteristic to redox progress of $LiMn_2O_4$ [24]. The relationship between discharge capacity retention and current density was plotted in Fig. 4(d). It should be mentioned that the capacity measured at low rate was a little higher than the maximum value for the 5 mC and 10 mC sample, but it is a reproducible phenomenon. A similar behavior was reported by Rougier et al. [25], and they explained that it was probably due to the interference from the interface between the film and current collector. Nevertheless, the

Table 1
The mass of the precursor and $LiMn_2O_4$ thin film and estimated thickness.

	f_0 (Hz)	f_{MO} (Hz)	Δf (Hz)	Δm (μg)	M_{LMO} (μg)	T (nm)
10 mC	5966396.942	5966124.267	272.675	4.458	2.968	9.26
20 mC	5971099.213	5970430.051	669.162	10.940	9.046	22.70
100 mC	5965172.500	5961761.095	3411.405	55.775	46.123	115.90

*The density of $LiMn_2O_4$ was estimated at 4.3 g cm^3. The f_0, f_{MO}, Δf, Δm, M_{LMO}, T represent resonant frequency of crystal electrode, frequency of crystal electrode deposited by manganese oxide precursor, frequency change, mass of deposited precursor, mass of estimated $LiMn_2O_4$, thickness of $LiMn_2O_4$ thin film, respectively.

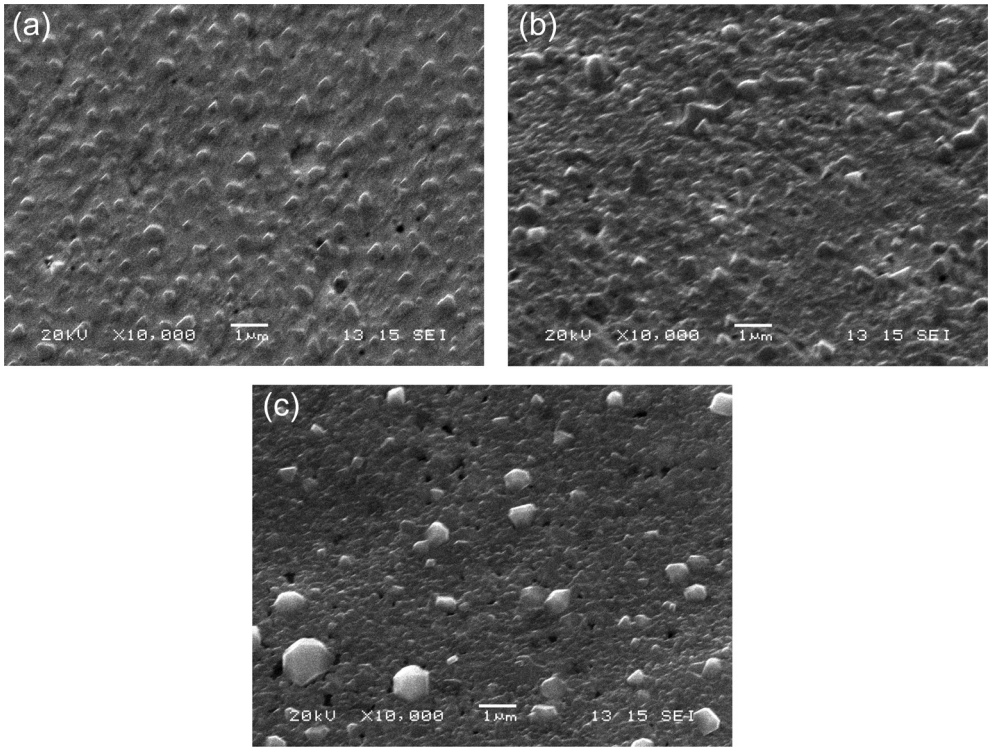

Fig. 3. SEM images of surface morphology for (a) 5, (b) 10, (c) 50 mC samples.

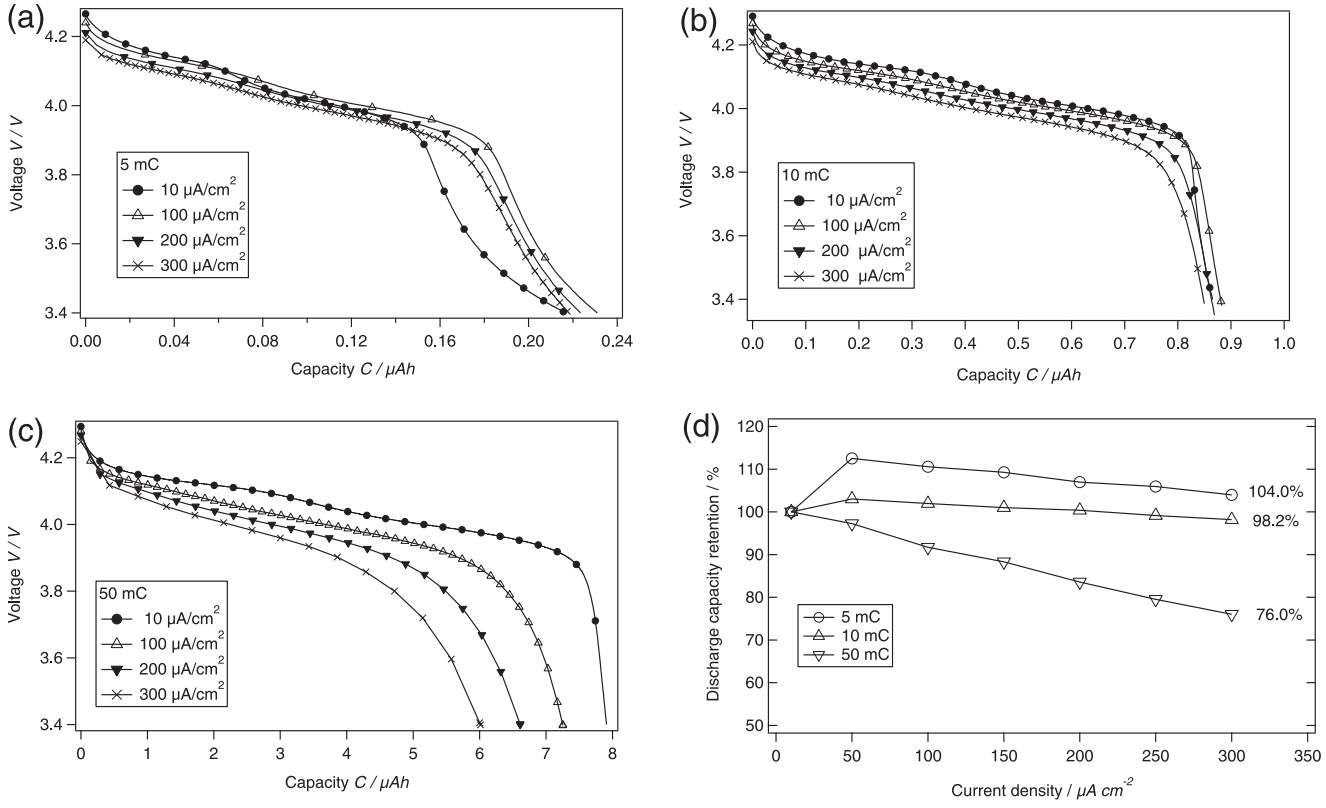

Fig. 4. The charge–discharge curves with various discharge current of $LiMn_2O_4$ on Au substrate. (a) 5 mC, (b) 10 mC, (c) 50 mC. (d) Relationship between discharge capacity retention and discharge current density.

5 mC and 10 mC showed excellent high rate discharge performance: 104% and 98.2% of discharge capacity retained when the current density increased from 10 to 300 μA cm^{-2}, respectively. The discharge capacity essentially unchanged from 10 μA cm^{-2} up to 300 μA cm^{-2} and the two plateaus still can be observed until at high current density of 300 μA cm^{-2} for the 5 and 10 mC samples. It has been widely acknowledged that the fade of the discharge capacity and disappearance of plateaus are due to the increasing cell polarization caused by lithium diffusion resistance with increasing in current density. This high capacity retention would be attributable to the small particle size of $LiMn_2O_4$ thin film with short Li^+ diffusion distance. For the thicker film of 50 mC sample, the discharge capacity was gradually decreased to 76% of the initial capacity with increasing the discharge current to 300 μA cm^{-2} and two plateaus tend to indistinct from the current of 200 μA cm^{-2}. From the capacity fading of 50 mC sample with the similar particle size of 50 nm, it can be conformed that the film thickness also play important role in high rate discharge performance in the case of film electrode owing to the increase in electric resistance. In addition, the lithium intercalation/deintercalation process requires longer time to reach the equilibrium for the thicker film because larger amount of materials are contained than thinner films [25]. In the present study, thickness of the films with 5 mC and 10 mC samples estimated from the theoretical mass of $LiMn_2O_4$ was only 9.26 nm and 22.7 nm, respectively. This theoretical thickness lower than the particle size suggests the rough surface of the film and this is consistent with the surface SEM image shown in Fig. 3. For the further investigation of the high rate discharge performance of the thin films, CV measurements were carried out.

Fig. 5(a–c) shows the cyclic voltammogram of $LiMn_2O_4$ thin films on Au substrates with various thickness recorded at the scan rate from 0.5 mV s^{-1} to 20 mV s^{-1}. The location of two peaks on charge and discharge are corresponding to the potential of plateaus. For the cyclic voltammetry plotted under the scan rate of 0.5 mV s^{-1}, the separation between a pair of peaks for three samples at 4.0 V is all about 30 mV. Previously, our group reported that the epitaxial $LiMn_2O_4$ thin film showed very small peak separation of 18 mV at the scan rate of 1 mV s^{-1} in the CV measurement associating to very low surface roughness, small grain boundary and ordered orientation [10]. Although the peak separation of the $LiMn_2O_4$ prepared in this work is a little bigger than epitaxial $LiMn_2O_4$ thin film, small ohmic drop in discharge curves and the high electric conductivity of the thin films are deserved for further electrochemical measurements [26].

It is well known that the change in peak shape with scan rate reflects the kinetics of Li^+ intercalation/deintercalation process. Well resolved reversible peaks both in the cathodic and anodic scan step until the high scan rate of 20 mV s^{-1} indicate good reversibility even at high rate redox reaction. Progressive shift of cathodic peaks in the discharge was observed with increasing scan rate v as well as in height. The relationship of peak current change at 4.0 V of cathodic scan (corresponding to the plateau region at 4.0 V) and the scan rate was in Fig. 5(d). For the thinner films of 5 and 10 mC samples, the cathodic current peaks increased in almost direct proportion to the potential sweep rate continued to 20 mV s^{-1}. This is typical behavior for the equilibrium at the intercalation electrode [5]. Comparatively, the peak current increased proportionally to square root of the scan rate $v^{1/2}$ for the 50 mC sample when the scan rate was faster than 10 mV s^{-1}, as shown in Fig. 5(d), which is characteristic of a solid state diffusion controlled situation [27]. Based on a square root linear relationship between the peak current and the scan rate in the diffusion controlled region (10–20 mV s^{-1}), diffusion coefficient of Li^+ into the 50 mC sample can be estimated from the classical Randles–Sevchik equation [28] as below,

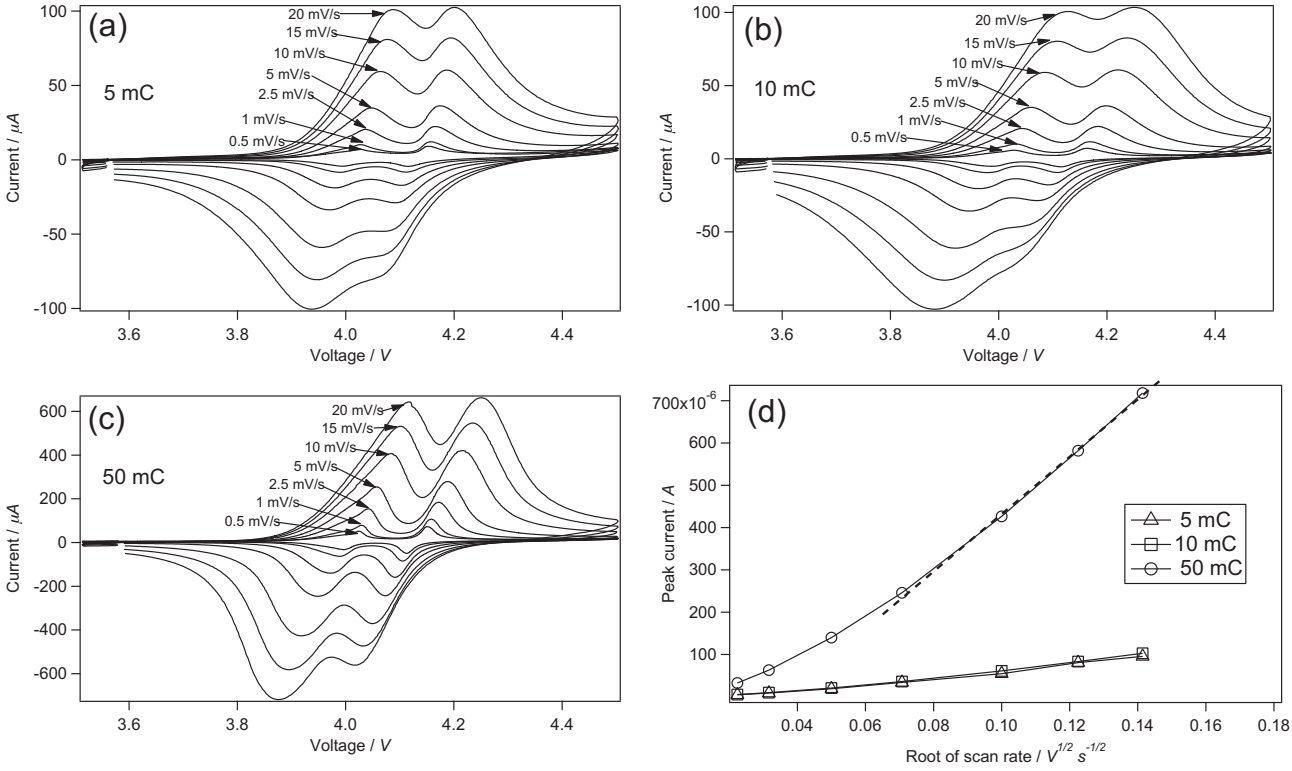

Fig. 5. Cyclic voltammetry curves of the $LiMn_2O_4$ at various scan rate of 0.5 mV s^{-1} to 20 mV s^{-1}. (a) 5 mC (b) 10 mC (c) 50 mC. (d) The relationship between peak current change at 4.0 V and the square root of scan rate. The broken line indicates the slop of $I_p \propto v^{1/2}$.

$$I_p = 0.4663FAC_R\left(\frac{nF\nu D}{RT}\right)^{1/2} \quad (4)$$

Where I_p is the peak current (A), F is the Faraday's constant, A is the surface area of the electrode (cm^2), C_R is the Li-ion concentration, n is the charge transfer number, R is the gas constant, T is the absolute temperature (K), D is the Li-ion chemical diffusion coefficient ($cm^2\ s^{-1}$), and the ν is the scanning rate ($V\ s^{-1}$). As a result, the Li ion chemical diffusion coefficient estimated by the Eq. (4) is $2.516 \times 10^{-9}\ cm^2\ s^{-1}$, which is higher than 10^{-10}–$10^{-11}\ cm^2\ s^{-1}$ for the $LiMn_2O_4$ thin film prepared by PLD method [23] and $4 \times 10^{-10}\ cm^2\ s^{-1}$ for r.f. sputtered $LiMn_2O_4$ films [29]. According to the previous reports, the chemical diffusion coefficient Li^+ ion in $LiMn_2O_4$ powder (ca. $10^{-9}\ cm^2\ s^{-1}$) [30] is higher than that at PLD or r.f.-sputtered $LiMn_2O_4$ thin film. The difference between the powder form and the thin film prepared by physical vapor deposition (PVD) technology was reported to caused by the difference in static disorder or short chains with undistorted 16*c*-8*a*-16*c* Li^+ ion diffusion pass [23]. In this work, the electrodeposited manganese oxide precursor was sintered at elevated temperature with LiOH to form $LiMn_2O_4$ thin film, which is consisted of nanoparticle. It is considered that the $LiMn_2O_4$ thin film synthesized by electrodeposition and subsequent sintering method has some feature of power form, including high Li^+ ion diffusion coefficient. Therefore, it is considered that the high diffusion coefficient and short diffusion length leaded to the high rate discharge capability.

Li ion diffusion coefficient in the 50 mC sample at 4.0 V was also estimated from electrochemical impedance spectroscopy. Nyquist plot in the frequency range of 10^6–10^{-2} Hz was shown in Fig. 6. A semi-circle in high-middle frequency region and a straight line about 45° slope in the low frequency region were observed. The semi-circle in the high-middle frequency would be attributed to charge-transfer resistance and the straight line is attributed to Warburg region that related Li^+ diffusion in the bulk $LiMn_2O_4$ thin film [26]. Therefore, the Nyquist plot can be fitted using equivalent circuit that composed of R_Ω: bulk resistance of electrode, R_{ct}: charge-transfer resistant, C_d: double-layer capacitance, Z_w: Warburg impedance as shown in inset of Fig. 6. The agreement of the solid line indicates the good fitting result. The chemical diffusion coefficient can be estimated from Eq. (5) [31]:

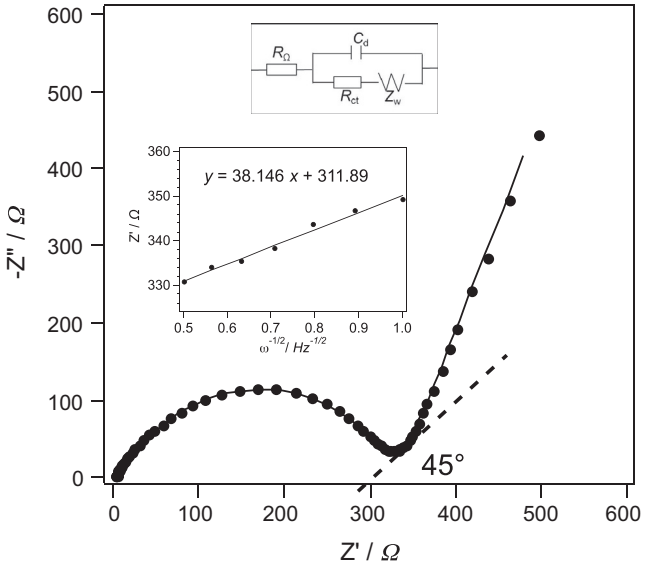

Fig. 6. The Nyquist plot of 50 mC sample at 3.996 V at the frequency range of 10^6–10^{-2} Hz (inset) the relationship between Z' and $\omega^{-1/2}$. The fitting model was also shown in inset.

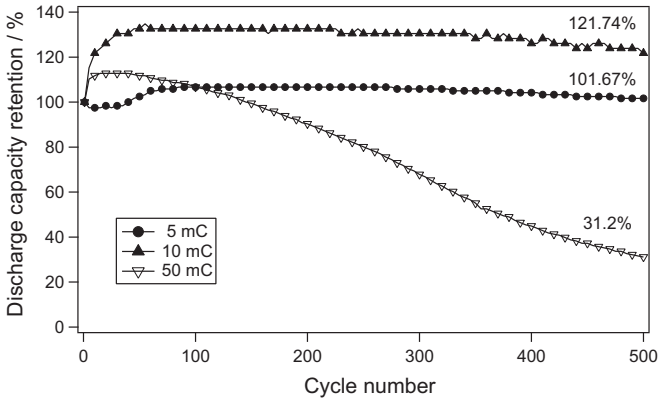

Fig. 7. The comparison of the cycle performance for the $LiMn_2O_4$ with various film thickness.

$$D_{Li} = \frac{1}{2}\left[\left(\frac{Vm}{FS\sigma}\right)\left(\frac{dE}{d\delta}\right)\right]^2 \quad (5)$$

Where Vm, F, S, σ and $dE/d\delta$ represent molar volume of $LiMn_2O_4$ ($cm^3\ mol^{-1}$), The Faraday's constant, the surface area of the electrode (cm^2), Warburg factor and slope of the electrode potential E vs composition δ (V), respectively. The Warburg factor σ can be obtained from slop of real impedance Z' and frequency $\omega^{-1/2}$ that plotted in inset of Fig. 6. The diffusion coefficient D_{Li} calculated from Eq. (5) is $1.49 \times 10^{-11}\ cm^2\ s^{-1}$. This value is two orders lower than the result of CV measurement. In this case, the chemical diffusion maybe contains some error due to the unclear Warburg region (not strictly 45°). Nevertheless, the chemical diffusion coefficient of 10^{-9}–$10^{-11}\ cm^2\ s^{-1}$ denoted high rate of the diffusion of Li ion in the bulk $LiMn_2O_4$ thin film.

The cyclability of $LiMn_2O_4$ thin films with various thickness was shown in Fig. 7. The charge–discharge was carried out at the voltage range of 4.3 V–3.6 V with the charge–discharge current of 50 $\mu A\ cm^{-2}$. It should be noted that, the thinner films of 5 and 10 mC samples showed superior cycle performance without capacity fading during 500 cycles, whereas the discharge retention of 50 mC sample gradually descend to 31.22%. As was reported by Tang et al. [32], the thinner films with comparatively lower crystallinity may be able to endure the mechanical stress due to the volume change during charge–discharge process and show good cyclability. On the other hand, the maximum capacity (135%) was obtained at 55th cycle for 10 mC sample at relatively low, constant discharge current, while the 5 mC sample retained almost 100% discharge capacity from the first cycle as shown in Fig. 7. In the CV curves (Fig. 5), 5 mC and 10 mC samples showed similar peak current although the different amount of active materials. Compared with 5 mC sample, it seems that the 10 mC need a little long charge–discharge cycle duration to reach 'fully activated state', especially at high discharge current. Unfortunately, the detail mechanism was uncertain, but it maybe due to two reasons, one is the interference from the interface between the film and current collector [25], the other is the existence of different amount manganese oxide impurity in the 5 mC and 10 mC samples that can be observed at XRD patterns at Fig. 1.

4. Conclusion

$LiMn_2O_4$ thin films with various thickness were prepared by sintering electrodeposited manganese oxide precursor on the Au substrate. The $LiMn_2O_4$ thin films composed of nanoparticles with

the size of 50 nm that independent from film thickness. In particular, thinner film derived excellent high rate performance and cyclability. Almost 100% of the capacity preserved when discharge current density is raised from 10 μA cm^{-2} to 300 μA cm^{-2} and showed superior cycle performance without capacity fading during 500 cycles. From the CV and EIS measurement, it is confirmed that the $LiMn_2O_4$ thin film has good electric conductivity with substrate and high lithium diffusion coefficient of 10^{-9}–10^{-11} cm^2 s^{-1}.

Acknowledgments

We thank Prof. Imanishi (Mie University) for the SEM measurements and Prof. Takada (Nagoya Institute of Technology) for the QCM measurements.

References

[1] M.M. Thackeray, W.I.F. David, P.G. Bruce, J.B. Goodenough, Mater. Res. Bull. 18 (1983) 461.
[2] R.J. Gummow, A. de Kock, M.M. Thackeray, Solid State Ionics 69 (1994) 59.
[3] Y.J. Park, J.G. Kim, M.K. Kim, H.T. Chung, W.S. Um, M.H. Kim, H.G. Kim, J. Power Sources 76 (1998) 41.
[4] Y.J. Park, J.G. Kim, M.K. Kim, H.T. Chung, H.G. Kim, Solid State Ionics 130 (2000) 203.
[5] M. Mohamedi, D. Takahashi, T. Itoh, M. Umeda, I. Uchida, J. Electrochem. Soc. 149 (2002) A19.
[6] N. Anzue, T. Itoh, M. Mohamedi, M. Umeda, I. Uchida, Solid State Ionics 156 (2003) 301.
[7] K.H. Hwang, S.H. Lee, S.K. Joo, J. Electrochem. Soc. 141 (1994) 3296.
[8] S. Komaba, N. Kumagai, M. Baba, F. Miura, N. Fujita, H. Groult, D. Devilliers, B. Kaplan, J. Appl. Electrochem. 30 (2000) 1179.
[9] M. Hirayama, N. Sonoyama, M. Ito, M. Minoura, D. Mori, A. Yamada, K. Tamura, J.i. Mizuki, R. Kanno, J. Electrochem. Soc. 154 (2007) A1065.
[10] N. Sonoyama, K. Iwase, H. Takatsuka, T. Matsumura, N. Imanishi, Y. Takeda, R. Kanno, J. Power Sources 189 (2009) 561.
[11] T. Matsumura, N. Imanishi, A. Hirano, N. Sonoyama, Y. Takeda, Solid State Ionics 179 (2008) 2011.
[12] J. Morales, L. Sanchez, S. Bijani, L. Martinez, M. Gabas, J.R. Ramos-Barrado, Electrochem. Solid State Lett. 8 (2005) A159.
[13] V. Georgieva, M. Ristov, Sol. Energy Mater. Sol. Cells 73 (2002) 67.
[14] I. Zhitomirsky, M. Cheong, J. Wei, JOM J. Minerals, Metals Mater. Soc. 59 (2007) 66.
[15] D. Zhao, Z. Yang, L. Zhang, X. Feng, Y. Zhang, Electrochem. Solid State Lett. 14 (2011) A93.
[16] L. My Loan Phung, L. Thi Xuan Binh, P. Quoc Trung, N. Thi Phuong Thoa, Adv. Nat. Sci. Nanosci. Nanotechnol. 2 (2011) 025014.
[17] S. Suzuki, K. Fujita, Y. Asami, F. Honma, JPN.Kokai Tokkyo Koho JP 61171062 (1986). A19860801.
[18] Z. Quan, K. Iwase, N. Sonoyama, J. Power Sources 196 (2011) 6762.
[19] D. Singh, R. Houriet, R. Giovannini, H. Hofmann, V. Craciun, R.K. Singh, J. Power Sources 97-98 (2001) 826.
[20] F. Cao, J. Prakash, Electrochim. Acta 47 (2002) 1607.
[21] F. Buciuman, F. Patcas, R. Craciun, D.R.T. Zahn, PCCP 1 (1999).
[22] T. Gao, H. Fjellvag, P. Norby, Anal. Chim. Acta 648 (2009) 235.
[23] C. Julien, E. Haro-Poniatowski, M.A. Camacho-Lopez, L. Escobar-Alarcon, J. Jimenez-Jarquin, Mater. Sci. Eng. B 72 (2000) 36.
[24] T. Ohzuku, M. Kitagawa, T. Hirai, J. Electrochem. Soc. 137 (1990) 40.
[25] A. Rougier, K.A. Striebel, S.J. Wen, E.J. Cairns, J. Electrochem. Soc. 145 (1998) 2975.
[26] I. Yamada, T. Abe, Y. Iriyama, Z. Ogumi, Electrochem. Commun. 5 (2003) 502.
[27] E. Levi, E. Zinigrad, H. Teller, M.D. Levi, D. Aurbach, E. Mengeritsky, E. Elster, P. Dan, E. Granot, H. Yamin, J. Electrochem. Soc. 144 (1997) 4133.
[28] J. Xie, N. Imanishi, T. Matsumura, A. Hirano, Y. Takeda, O. Yamamoto, Solid State Ionics 179 (2008) 362.
[29] K.H. Hwang, S.H. Lee, S.K. Joo, J. Power Sources 54 (1995) 224.
[30] A. Dell'Era, M. Pasquali, J. Solid State Electrochem. 13 (2009) 849.
[31] C. Ho, I.D. Raistrick, R.A. Huggins, J. Electrochem. Soc. 127 (1980) 343.
[32] S.B. Tang, M.O. Lai, L. Lu, Electrochim. Acta 52 (2006) 1161.